The role and analysis of molecular systems in electrocatalysis

Dijk, B. van

Chapter 4

A selective molecular dinuclear copper oxygen reduction catalyst for the electrochemical synthesis of H_2O_2 at neutral pH

*H_2O_2 is a bulk chemical used in a variety of applications as, for example, bleaching, or as a disinfecting agent. The anthraquinone process is the sole bulk production method of H_2O_2 which inherently has a negative effect on the energy and cost requirements as various purifications steps are required. The electrochemical O_2 reduction to H_2O_2 is viable alternative with examples of the direct production of up to 20% H_2O_2 solutions. We found that H_2O_2 over-reduction was significantly blocked for the dinuclear copper complex **Cu_2(btmpa)** (btmpa = 6,6'-bis[[bis(2-pyridylmethyl)amino]methyl]-2,2'-bipyridine) due to slow electron transfer in the Cu^{II} to Cu^{I} reduction. Electrochemically, **Cu_2(btmpa)** was found to reduce O_2 with a selectivity in the start of a measurement up to 90% towards H_2O_2 according to rotating ring disk electrode (RRDE) measurements. Quartz crystal microbalance measurements showed that reduction of the complex leads to an adsorption on the electrode. This adsorption results in accumulation of active sites on the carbon electrode thereby increasing the O_2 reduction current from –0.2 to –0.4 mA at 0.0 V which is close to the theoretical diffusion limited current. In addition, the Faradaic efficiency for H_2O_2 remained up to 60 to 70% for 2 hours during chronoamperometry experiments at 0.0 V as was determined by periodic enzyme based photometric measurements. After 2 hours, rising concentrations of H_2O_2 intensify Cu^0 deposition that progressively lowers the Faradaic efficiency by over-reduction of H_2O_2. Nevertheless, we found that the efficiency can be improved by introducing high potential intervals to strip Cu^0. Moreover, we showed that H_2O_2 interception by re-oxidation in a RRDE setup plays an important role in tempering Cu^0 deposition. Fine-tuning the operating potential, interval timing and being able to intercept formed H_2O_2 all could help to retain the high Faradaic efficiency. For the first time, extensive studies into the long term electrochemical O_2 to H_2O_2 reduction by a molecular complex have been performed which allowed to retain the high intrinsic selectivity of **Cu_2(btmpa)** towards electrochemical H_2O_2 production.*

The results in this chapter are to be submitted as: B. van Dijk, R. Kinders, D. G. H. Hetterscheid, *A selective molecular dinuclear copper oxygen reduction catalyst for the electrochemical synthesis of H_2O_2 at neutral pH*

4.1 Introduction

H_2O_2 is a bulk chemical that is produced on a 4.5 million ton scale[1] and used in many applications[2] such as bleaching (largest single use),[3, 4] waste water treatment,[5, 6] disinfecting, and industrial organic synthesis.[7] It is one of the most environmentally friendly chemical oxidants because the decomposition products are water and/or O_2. Moreover, up to 50% of the oxygens in H_2O_2 are used in the oxidation thereby enhancing the atomic efficiency with respect to other chemical oxidations such as $NaIO_4$ and *t*BuOOH.[8] Even though H_2O_2 is considered as environmentally friendly, its current production method is certainly not. Over 90% of the worldwide H_2O_2 production is via the anthraquinone process.[2, 8] Here, anthraquinones are used as redox mediators that first undergo reduction with H_2, followed by a separate re-oxidation in the presence of air (O_2) which produces H_2O_2 selectively. Liquid-liquid extractions are required to extract H_2O_2 given that these reactions take place in organic solvent. Consequently, the obtained H_2O_2 is contaminated with organic impurities. As a result, most of the cost and energy of producing H_2O_2 result from the purification of this extract.

The electrochemical reduction of O_2 to H_2O_2 is a viable alternative for the anthraquinone process and was first reported in 1939 by Berl.[9] In fact, it has been industrialized in the Huron-Dow process which is mostly used for on-site production of alkaline peroxide mixtures for the paper bleaching industry. Nevertheless, this only covers a negligible fraction of the total H_2O_2 production.[2, 8] To overcome the problem of separating the H_2O_2 from the aqueous electrolyte, solid electrolyte cells in combination with flow cell chemistry have recently been proposed as a feasible option.[10] Specifically, H_2O_2 solutions up to 20% with higher purity than the anthraquinone process could be directly obtained. The cathode, where O_2 reduction takes place, can be made of several materials. Noble metals are usually not the best choice since they either catalyze the full 4 electron reduction to H_2O, or they interact weakly with O_2 resulting in low rates and a high overpotential.[11] Attempts to combine these characteristics in alloys have resulted in better catalysts,[11] such as Pt–Hg,[12] Pd–Hg,[13] and Pd–Au[14] alloys. Another interesting approach is the use of carbon based catalysts. In general, carbon electrodes have an intrinsic selectivity towards the formation of H_2O_2 when performing O_2 reduction.[15] Their reactivity is however quite poor, and application of such materials therefore requires large overpotentials.[11] Improvements can be made by increasing the defect[16, 17] and/or oxygen content,[18, 19] doping with heteroatoms,[20-23] or doping with metals as single-site catalysts. For the latter, molecular complexes can help to establish good adsorption through ligand-

carbon interactions because metal–support interactions for carbon are relatively weak.[11] Most molecular catalysts, that have been reported to perform the reduction of O_2 to H_2O_2, have only been studied in non-aqueous solvents.[24-26] Mechanisms and selectivity depend significantly on the acid type and acid strength and cannot be directly translated to aqueous solutions. Until now, high selectivity for electrocatalytic H_2O_2 production in aqueous solutions is observed only for a few manganese,[27, 28] iron,[29-32] copper,[28, 33] and cobalt complexes.[28, 32, 34-39] The initial high selectivity is often restricted to a small potential window and only observed for a few minutes. Longer measurements are often not performed. If performed, they typically result in an overall 4 electron selectivity either due to over-reduction of H_2O_2 or due to the disproportionation of H_2O_2, also catalyzed by these molecular catalysts.[30] Thus far, there is only one exception of a cobalt tetrakis(*N*-methyl-4-pyridyl)porphyrin complex that was reported with high selectivity (>90%) for H_2O_2 after 2 hours of electrolysis, but apart of this claim no further details were provided.[34]

Our group reported $[Cu(tmpa)(L)]^{2+}$ (**Cu(tmpa)**, Chart 4.1, tmpa = tris(2-pyridylmethyl)amine, L = solvent) for the electrochemical 4 electron reduction of O_2 to H_2O that proceeds in a stepwise mechanism with H_2O_2 as detectable intermediate.[33] At pH 7, two separate catalytic cycles for O_2 to H_2O_2 and H_2O_2 to H_2O reduction take place with onsets of 0.50 and 0.45 V *versus* the reversible hydrogen electrode (RHE), respectively. The suggested O_2 to H_2O_2 reduction mechanism starts with coordination of O_2 to a reduced Cu^{I} complex resulting in the previously reported end-on copper superoxo complex.[40, 41] Subsequently, a PCET (proton coupled electron transfer) most likely results in formation of a hydroperoxo complex and is followed by a proton transfer to produce H_2O_2. Further reduction of H_2O_2 most likely takes place by Fenton type chemistry which splits H_2O_2 in a copper bound hydroxyl and free hydroxyl radical.[42, 43] Both the reduction of O_2 and H_2O_2 are very fast and mass transport limited in oxygen at almost all conditions. For that reason, high selectivity for H_2O_2 can only be observed close to the onset potential of the reduction of O_2 to H_2O_2. At more negative potentials, the formed H_2O_2 is over-reduced to H_2O.

Even though **Cu(tmpa)** is an intrinsic very fast catalyst for the O_2 to H_2O_2 reduction, the over-reduction of H_2O_2 is equally fast limiting the applicability for H_2O_2 production. For that reason, we set out to investigate **Cu_2(btmpa)** (Chart 4.1): the dicopper complex $[Cu_2(btmpa)(L)_4]^{4+}$ (btmpa = 6,6'-bis[[bis(2-pyridylmethyl)amino]methyl]-2,2'-bipyridine) which is consisting of two **Cu(tmpa)** moieties fused via a covalent bond between one of the three pyridines on each moiety resulting in a bipyridine backbone.[44-46] An earlier report suggested that

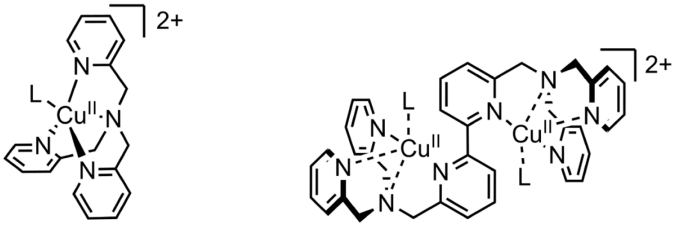

Cu(tmpa) **Cu_2(btmpa)**

Chart 4.1. Structures of **Cu(tmpa)** and **Cu_2(btmpa)**.

the Cu^I complex of **Cu_2(btmpa)** had diminished reactivity towards O_2 with respect to **Cu(tmpa)** since an O_2 purged solution of **Cu_2(btmpa)** only showed a very slow color change over the course of several hours.[46] Also, the $Cu^{I/II}$ redox couple potential had shifted positively with respect to **Cu(tmpa)** in organic solvents indicating that the Cu^I state was thermodynamically more favorable. Moreover, the geometry of the Cu^I complex was significantly different from the Cu^I complex of **Cu(tmpa)** as was concluded from ^1H NMR data. As these properties could influence the electrochemical O_2 and H_2O_2 reduction significantly, we were interested whether H_2O_2 selectivity could be improved. Indeed, we found that H_2O_2 reduction was mostly inhibited resulting in a high selectivity for H_2O_2. In addition, we performed for the first time a systematic study of long bulk electrosynthesis of H_2O_2 by a molecular catalyst. By performing long amperometry measurements, we were able to identify factors that limit the Faradaic efficiency, improve the process, and thereby achieve up to 70% Faradaic efficiency for H_2O_2 over the course of 2 hours.

4.2 Results and Discussion

4.2.1 Synthesis, magnetic properties, and electrochemistry

The dinucleating btmpa ligand was synthesized by the S_N2 reaction of 6,6'-(dichloromethyl)-2,2'-bipyridine (**4**) and commercially available 2,2'-dimethylpyridylamine (dmpa) following literature proceedings.[45] The earlier reported synthesis was slightly adjusted by using **4** which bears a chloromethyl instead of bromomethyl moiety (Scheme 4.1). We found that unreacted dmpa was hard to remove by common chromatography methods as both btmpa and dmpa display significant tailing. Therefore, an additional purification method was developed to improve the yield of pure btmpa (for details, see the experimental section). In short, dmpa is selectively converted to an amide by adding hexanoic

anhydride to the crude mixture of dmpa and **4**. This amide can easily be removed by chromatography methods and btmpa was successfully purified with a yield of 21%. Next, the Cu^{II} complex was synthesized by mixing a solution of $Cu^{II}(CF_3SO_3)_2$, and btmpa. After recrystallization by vapor diffusion of diethyl ether in a methanolic solution, blue colored crystals of the complex were obtained with 63% yield with $[Cu_2(btmpa)(CH_3OH)_2](CF_3SO_3)_4$ as molecular formula determined by elemental analysis. Neutral aqueous solutions containing **Cu_2(btmpa)** are blue colored arising from a broad Cu^{II} d-d transition at 675 nm (Figure C.1).

Cu_2(btmpa) has two copper centra which could interact with each other. A possible magnetic interaction between the copper centra can be investigated with EPR (electron paramagnetic resonance) and SQUID (superconducting quantum interference device) spectroscopy. From fitted SQUID data, a small (ferromagnetic) coupling of 34 cm^{-1} was found and EPR did not show any evidence for large coupling between both copper centers (Figures C.2 and C.3). Another interesting aspect of the dinuclear complex is the equilibrium potential of the $Cu^{I/II}$ redox couple of the two copper centers in aqueous solutions. Previous electrochemical studies of **Cu_2(btmpa)** in organic solvents suggested that the two copper centers are reduced simultaneously because only one redox couple was observed. In addition, their equilibrium potential shifted positively with respect to the mononuclear **Cu(tmpa)**.[46] Therefore, cyclic voltammetry (CV) under an argon atmosphere in a pH 7 phosphate buffer was performed. This revealed only one redox wave for the Cu^{I}/Cu^{II} redox couple (Figure 4.1A) at 0.51 V *versus* the Reversible Hydrogen Electrode (RHE). Interestingly, the $E_{1/2}$ of the redox couple of **Cu_2(btmpa)** has shifted 0.30 V positively with respect to **Cu(tmpa)**. A previously published crystal structure of a $[(btmpa)Cu_2(CH_3\text{-}CN)_2(ClO_4)_2]^{2+}$ complex showed that the Cu–N bond

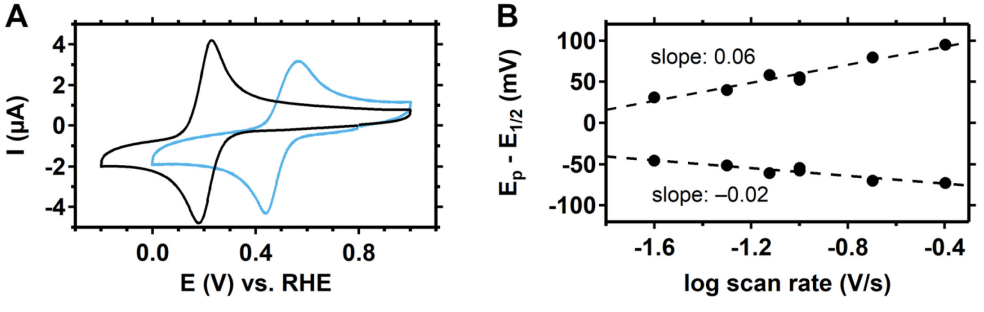

Figure 4.1. (A) Cyclic voltammogram of a 0.15 mM **Cu_2(btmpa)** solution (blue) and a 0.3 mM **Cu(tmpa)**[33] solution (black) under an argon atmosphere in a 0.1 M phosphate buffer of pH 7 with a scan rate of 100 mV/s. (B) Laviron plot of the cathodic and anodic peak positions of **Cu_2(btmpa)** and the slopes of linear fits.

of the bipyridine moiety has longer distances (2.4 Å) than the other pyridines (2.0 Å).[46] As a result, the Cu^{II} site is less electron dense than **Cu(tmpa)** which explains the positive shift of the $Cu^{I/II}$ redox couple. The $Cu^{I/II}$ redox couple has a large peak separation of 0.12 V at 100 mV/s scan rate. Varying the scan rate did not reveal a second redox couple, but instead revealed that the peak separation increases with increasing scan rate (Figure 4.1B). This points to a relative slow electron transfer process due to restricted reorganization of the geometry of **Cu_2(btmpa)** when reduced and re-oxidized. In contrast, the reduction of the mononuclear **Cu(tmpa)** complex is a very fast process[33] due to the easy transition of a trigonal bipyramidal geometry of the Cu^{II} complex to the preferred tetragonal geometry for the Cu^{I} state by the elongation of Cu–N distance of the tertiary amine from 2.10 to 2.43 Å.[47] In contrast, the Cu^{II} geometry of **Cu_2(btmpa)** leans towards a pseudo-octahedral geometry.[46] As mentioned in the introduction, the **Cu^{I}_2(btmpa)** geometry was shown to be different from **Cu^{I}(tmpa)** according to ^{1}H NMR data.[46] Therefore, it seems unlikely that **Cu_2(btmpa)** can easily obtain the preferred tetragonal geometry for the Cu^{I} state which hinders fast electron transfer as would also be expected from the Marcus theory in which a higher reorganization energy is linked to slower electron transfer.[48]

Whereas **Cu(tmpa)** was found to be a homogeneous complex under electrochemical conditions,[33] **Cu_2(btmpa)** has a tendency to adsorb on the electrode. This behavior was studied in detail with electrochemical quartz crystal microbalance (EQCM) studies. EQCM is an *in-situ* technique that probes the mass changes of the work electrode by monitoring the change in oscillation frequency of the quartz crystal on which the work electrode resides.[49-52] In EQCM, a negative difference in frequency corresponds to an increase of the mass of the electrode. This technique visualizes any permanent deposit on the electrode as is sometimes formed by molecular complexes (see also Chapters 2 and 3).[49-52] Specifically, a gold electrode on such a quartz crystal was used for this purpose (Figure 4.2). The relative frequency of the oscillation decreases as soon as the complex is reduced electrochemically in the absence of O_2 starting at 0.5 V while scanning negative. In the positive scan, the complex is re-oxidized above 0.5 V which is accompanied by an increase of the frequency back to the starting frequency. Hence, the $Cu^{I/II}$ redox couple triggers a reversible change in mass of the electrode. This illustrates that no permanent deposit is formed. The origin of the reversible adsorption might be due to a change in solubility of the complex when changing the charge from 4+ to 2+. The less-charged complex could subsequently adsorb on the electrode more readily.

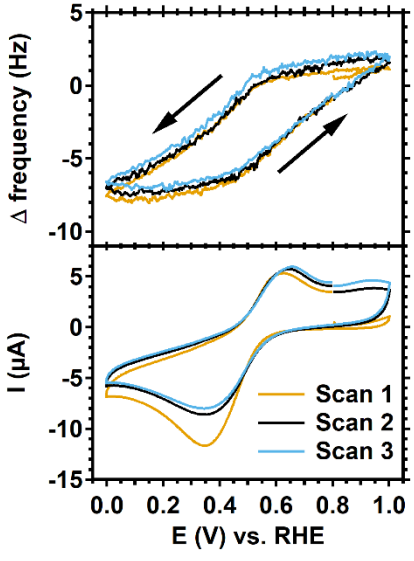

Figure 4.2. Electrochemical quartz crystal microbalance measurement with a gold work electrode of 0.15 mM **Cu_2(btmpa)** in 0.1 M phosphate buffer of pH 7. The bottom panel shows CV cycles at 50 mV/s scan rate under argon atmosphere. The first scan deviates because not all oxygen was completely removed. The top panel shows the relative frequency of the quartz crystal and its response with respect to the applied potential.

4.2.2 O_2 reduction by **Cu_2(btmpa)**

The electrochemical oxygen reduction reaction (ORR) of **Cu_2(btmpa)** was studied by cyclic voltammetry (CV) with a rotating ring disk electrode (RRDE) setup. This setup allows for controlled mass transport due to continuous rotation of the electrode resulting in a laminar flow of O_2 purged electrolyte towards the electrode. Furthermore, a Pt ring around the work electrode can be used as electrochemical sensor for the oxidation of H_2O_2 by applying a potential of 1.2 V. The onset for ORR for the glassy carbon (GC) work electrode itself is at *circa* 0.35 V *versus* RHE under our conditions (Figure 4.3). Generally, polished carbon electrodes such as GC selectively perform the 2 electron reduction of O_2 to H_2O_2.[15] Indeed, the production of H_2O_2 could be derived from the increase in ring current as soon as O_2 was reduced (Figure 4.3). When **Cu_2(btmpa)** was present in solution under an argon atmosphere, the onset for complex reduction was at 0.50 V. In addition, a ring current was observed which corresponds to the re-oxidation of the **Cu^I_2(btmpa)** at 1.2 V. When the solution was saturated with O_2, the onset lies at 0.50 V as well. However, the disk current exceeded the current in absence of O_2 pointing to the fact that catalytic O_2 reduction took place. Likewise, the ring current exceeded the current

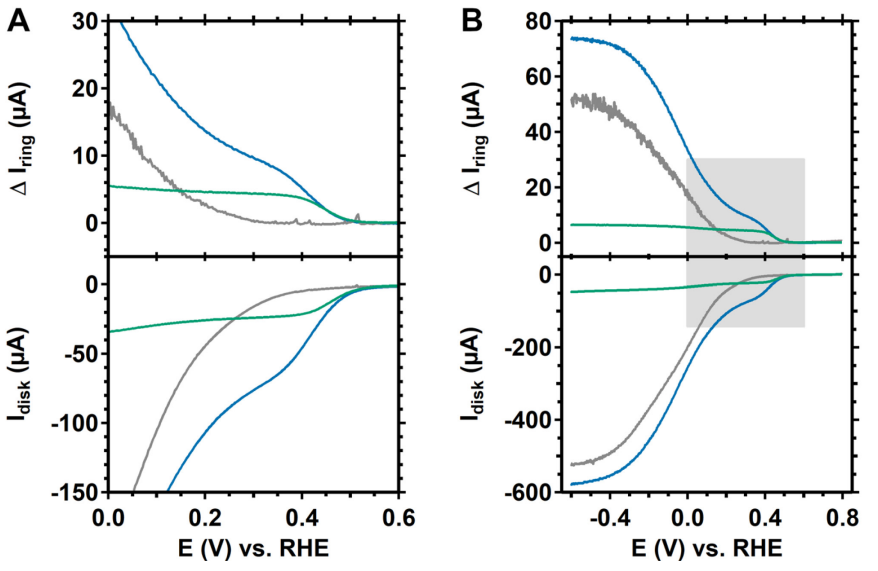

Figure 4.3. Linear sweep voltammograms with a rotating ring disk electrode setup of 0.15 mM **Cu_2(btmpa)** under argon (green) and O_2 atmosphere (blue). The cyclic voltammogram of the GC disk (bottom panel) and the current response of the Pt ring (top panel) are shown. The grey line represents the GC disk in catalyst-free, O_2 purged electrolyte. B shows the full potential window. The voltammograms were recorded at 50 mV/s in a 0.1 M phosphate buffer of pH 7. A rotation rate of 1600 rpm and a Pt ring potential of 1.2 V were applied.

in absence of O_2 indicating that H_2O_2 is formed. In the potential window between 0.50 and 0.35 V, the GC electrode itself is not active for O_2 reduction. Hence, **Cu_2(btmpa)** must perform O_2 reduction and produce H_2O_2. Below 0.35 V, the disk (and ring) current increased significantly because GC reduces O_2 as well in this potential window and a diffusion limited current was reached at −0.6 V. In this potential window, O_2 reduction is mostly performed by GC. Also, the diffusion limited current in presence of **Cu_2(btmpa)** is reached at the same potential as in the absence of **Cu_2(btmpa)**. **Cu_2(btmpa)** clearly reduces O_2 slower as compared to the mononuclear complex **Cu(tmpa)** as the latter reaches a diffusion limited current at 0.2 V.[33] The slow O_2 reduction of **Cu_2(btmpa)** is most likely due to the relative slow electron transfer kinetics of the $Cu^{I/II}$ redox couple.

4.2.1 H_2O_2 selectivity

The RRDE CV of O_2 reduction by **Cu_2(btmpa)** suggested that O_2 is reduced to H_2O_2 based on the observed ring current (Figure 4.3). To quantify the H_2O_2 selectivity, chronoamperometry at a fixed potential was performed. To calculate the H_2O_2 selectivity, the collection efficiency of the ring (N_{CE}) is required. Usually, the

one-electron redox couple $[Fe^{II}CN_6]^{4-}/[Fe^{III}CN_6]^{3-}$ is studied for this purpose, but this is not a good reference for multi-electron redox reaction such as H_2O_2 oxidation that includes the formation and breaking of bonds. In that case, the platinum ring is a catalyst whose activity is very susceptible for deactivation. To elaborate, the H_2O_2 oxidation mechanism on Pt is dependent on the number of active sites. This number can be reduced by competition of the phosphate buffer and PtO_x formation during a measurement when applying a potential of 1.2 V. In addition, substrate inhibition decreases H_2O_2 oxidation on Pt at high H_2O_2 concentration.[53] Moreover, we found that the polish method influences the activity of Pt and thereby the N_{CE} value. More information can be found in Appendix C (Figure C.4 and C.5). In short, mechanical polish with silica or alumina slurries will lower the N_{CE} for H_2O_2. A N_{CE} of 12.5% was previously determined under these conditions.[33] When the Pt ring is electropolished as well, the N_{CE} can reach the theoretical maximum value of 22-24% (depending on the ring-disk setup), but will quickly drop during a measurement which leads to a large inaccuracy. Therefore, we did not electropolish the Pt ring and determined the N_{CE} prior to the measurement by performing O_2 reduction with freshly polished GC disk and Pt ring electrodes at −0.3 V in a catalyst-free electrolyte. Since GC is a 100% selective catalyst for H_2O_2,[15] the obtained ring to disk current ratio was used as the N_{CE}.

Chronoamperometry in presence of **Cu_2(btmpa)** was performed at 0.2 V (Figure 4.4). The influence of O_2 reduction by GC is minimized at this potential (Figure 4.3). This establishes a reference for the intrinsic selectivity of **Cu_2(btmpa)** up to 15 minutes. A N_{CE} of 17.5% was determined and used to calculate the% H_2O_2 for this measurement (Figure 4.4B). As expected, the selectivity for H_2O_2 is high as the selectivity starts at 90% but lowers to 70% after 15 minutes. A selectivity below 100% suggests that over-reduction of H_2O_2 takes place. For that purpose, H_2O_2 reduction by **Cu_2(btmpa)** under argon atmosphere was studied (Figure C.6) with non-rotating and rotating electrodes. H_2O_2 is indeed reduced by **Cu_2(btmpa)** and the reducing current do increase with the H_2O_2 concentration. However, the H_2O_2 reduction by **Cu_2(btmpa)** is very sluggish which explains the high selectivity for H_2O_2.

4.2.2 Long-term electrolysis

Over-reduction or disproportionation of H_2O_2 is found for most molecular complexes that have been studied over a longer period of time. Also, catalyst degradation might play a role after a few hours. As was also mentioned in Chapter 1, a very small amount of unchelated copper is present since it is in equilibrium with

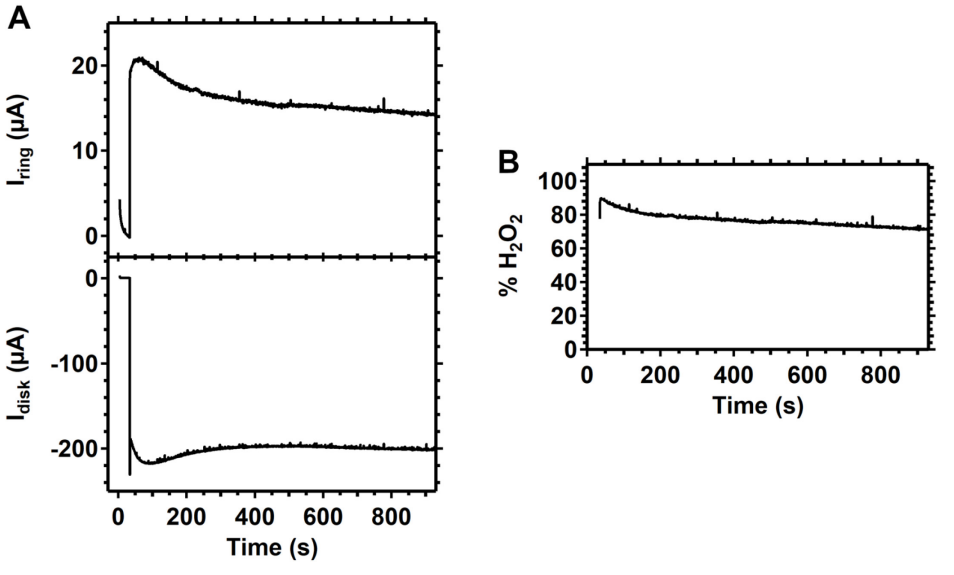

Figure 4.4. Chronoamperometry with a RRDE setup (A) of O_2 reduction in presence of **Cu_2(btmpa)** at 0.2 V disk potential (bottom panel) and corresponding Pt ring current (top panel). The calculated H_2O_2 selectivity is shown in B. A 0.1 M phosphate buffer at pH 7 with 0.15 mM catalyst was used. The GC disk was rotated at 1600 rpm. The Pt ring was kept at 1.2 V. The collection efficiency was determined at 17.5% determined by a 3 minute amperometry measurement at –0.3 V in catalyst-free electrolyte.

the chelated copper complex. At low, reductive potentials, this unchelated copper can be deposited as Cu^0 on the electrode. In contrast to most metals, copper has very fast ligand exchange rates. Hence, the tiny amount of unchelated copper is quickly replenished to re-establish the equilibrium with the copper complex. Consequently, the irreversible deposition of Cu^0 may very quickly pull the equilibrium towards dissociation of significant amounts of copper. The pace of the deposition could be influenced by the binding strength of the complex and/or the applied potential.[50, 51] To study these effects, O_2 reduction with **Cu_2(btmpa)** was monitored over a >7 hour period in O_2 saturated phosphate buffer. To do so, a rotating disk setup was used for constant diffusion of O_2 saturated electrolyte at 1600 rpm rotation rate. We chose 0.0 V as the most ideal potential because a background hydrogen evolution reaction was not expected, background O_2 reduction reactions on GC were minimal, and significant currents were generated at this potential in presence of **Cu_2(btmpa)**. Three different types of measurements were performed (Figure 4.5). First, a GC electrode in absence of **Cu_2(btmpa)** was tested as blank measurement (grey line). Second, a GC electrode in 0.15 mM catalyst solution was tested while continuously applying 0.0 V (green line). Last, a GC electrode in catalyst solution was tested with

intervals (orange): after 20 minutes of 0.0 V, the potential at the disk was briefly set at 0.8 V for 4 minutes (see the scheme in the top panel of Figure 4.5). The purpose of the interval measurement was to strip any (possible) Cu^0 deposition by briefly applying an oxidizing potential. Of note, H_2O_2 is not re-oxidized to O_2 at this potential (Figure C.6). The results of the continuous measurements with and without catalyst present show that the current is significantly higher in the presence of **Cu_2(btmpa)** (–0.25 mA *versus* –0.05 mA in the first minutes) and increases gradually over the course of 8 hours. In the first half hour, there is a large increase in current from –0.25 to –0.37 mA. This feature of quick increase within the first 30 minutes of the measurement is observed in all cases when catalyst is present but not in absence of the catalyst. Most likely, **Cu_2(btmpa)** accumulates on the electrode. At 0.0 V, O_2 reduction by **Cu_2(btmpa)** is still kinetically limited (Figure 4.3). As a result, the large increase in reductive current can be explained by an increase in active sites due to accumulation of the catalyst. The EQCM measurements hinted towards this behavior as there is some reversible, potential dependent adsorption on gold electrodes (Figure 4.2). Interestingly, the magnitude of the current at 0.0 V after a 4-minute 0.8 V interval is equal to what it ended at the preceding 20 minute amperogram. This indicates that the accumulation effect lasts on the GC electrode even when a potential of 0.8 V is applied. Only thoroughly rinsing the electrode could remove most of the adsorbed catalyst and lower the O_2 reduction current to the same level of GC in catalyst-free electrolyte (see Figure C.7).

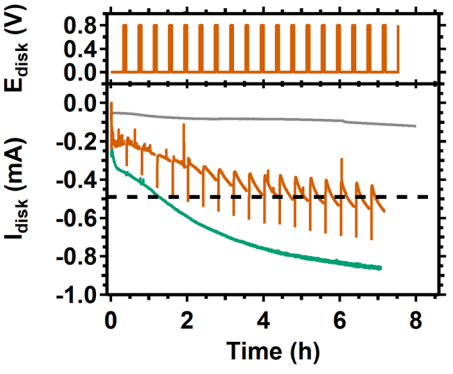

Figure 4.5. Rotating disk chronoamperometry of a GC disk at 0.0 V in a O_2 saturated **Cu_2(btmpa)** solution (bottom panel) in a continuous measurement (green) or a 20 minute interval measurement (orange). For the latter, a 0.8 V potential was briefly applied to re-oxidize accumulated Cu^0 deposition every 20 minutes according to the sequence shown in the top panel. The large negative spikes in the bottom panel are an artefact of these intervals. The grey line is a continuous experiment in absence of **Cu_2(btmpa)**. The dotted horizontal line represents the theoretic maximum current for the 2-electron O_2 reduction reaction. The disk was rotated at 1600 rpm in a 0.1 M phosphate buffer of pH 7 with 0.15 mM catalyst.

After 1.5 hours, the reducing current of the continuous measurement became close to the calculated diffusion limited current (−0.49 mA) for O_2 to H_2O_2 reduction under these conditions. The calculation is based on the diffusion limited current that a Pt disk of the same size (0.196 cm^2) reaches under the same conditions for the 4 electron reduction of O_2 to H_2O, for which −0.98 mA was obtained.[33] However, the current passed −0.49 mA after 1.5 hours and continued to rise even more. After the full 7 hour continuous measurement, the electrode was taken from the solution and a brown-colored deposit could be observed on the surface of the electrode (Figure C.8). Most likely, this is a Cu^0 deposit. As we will show later, this Cu^0 deposit can be linked to a gradual shift in selectivity from O_2 to H_2O_2 to the 4 electron reduction of O_2 to H_2O which requires more electrons and thus higher currents. Clearly, Cu^0 deposition is undesired and that is the reason for performing the interval measurement. During this measurement (orange line of Figure 4.5), the potential was held at 0.8 V for 4 minutes after every 20 minutes of catalytic amperometry at 0.0 V. Evidently, the current is lower as compared to the continuous measurement. Still, the current steadily increased over time. For the first 2 hours, the current at the start of every 20 minute cycle was of the same magnitude as that of the end of the previous cycle. After 2 hours, this was no longer the case. At that point, the current jumped back to a lower value after the interval than the magnitude it reached during the preceding cycle. Cu^0 deposition and the accompanying selectivity change could be the underlying reason as this would explain why the current jumps back after the stripping potential was applied. The observation that this happens after 2 hours might be related to a rise in the H_2O_2 concentration as we will discuss next. Overall, the interval procedure clearly prevented Cu^0 deposition to a certain extent with respect to a continuous measurement.

4.2.3 Faradaic efficiency for H_2O_2

The selectivity of **Cu_2(btmpa)** at 0.0 V for H_2O_2 over a prolonged period of time was monitored to study the effect of over-reduction of H_2O_2 by either **Cu_2(btmpa)** or Cu^0 deposition. Two different methods were used. The first method used the same RRDE set-up as for Figure 4.4 that utilizes the Pt ring as electrochemical H_2O_2 sensor. Here, we found that the ring is not suited as quantitative peroxide sensor during long-term electrolysis (see Figure C.9). As mentioned before, catalytic H_2O_2 oxidation by the Pt ring is very susceptible for deactivation by PtO_x formation and high amounts of H_2O_2 (Figures C.4 and C.5).[53] However, the data did suggest that there was a slow build-up of H_2O_2. Therefore, we applied a second method: bulk electrolysis with an RDE setup for which the bulk

concentration of H_2O_2 was periodically determined with an enzyme based photometric analysis using a reflectometer. The products of H_2O_2 dissociation by a peroxidase will react with an organic dye. The intensity of the color that arises can be used to quantify H_2O_2. Thereby, the Faradaic efficiency could be calculated which is the percentage of charge passing the disk that is used for the O_2 to H_2O_2 reduction.

The Faradaic efficiency was determined for three measurements with long (4 minute), short (30 seconds) and no intervals of 0.8 V. The results of the 4-minute interval measurement are shown in Figure 4.6. Within the first 30 minutes, a Faradaic efficiency of 83% was obtained which is in good agreement with the data obtained from the short-term RRDE experiment at 0.2 V (Figure 4.4). Likewise, in a continuous measurement without intervals, an efficiency of 80% was found after the first 30 minutes (Figure C.10). The measurement with shorter interval times had a lower Faradaic efficiency of 62% after 30 minutes, though a very noisy amperogram might have influenced this result (Figure C.10). Within the first half hour, the selectivity for H_2O_2 is high and the influence of Cu^0 deposition is clearly low. After the first half hour, the Faradaic efficiency of the 4-minute interval measurement lowered to around 60%. The shorter interval measurement had a slightly higher efficiency of 69%. In contrast, the continuous measurement showed a drastic drop in efficiency to 40% 1 hour after the start and stagnated around 10% after 2 hours. The interval experiments kept at 60 to 70% in the same time window clearly

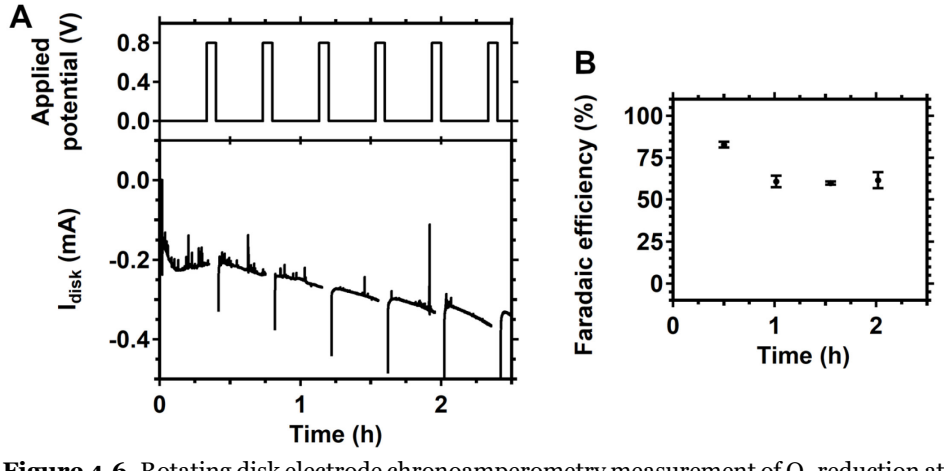

Figure 4.6. Rotating disk electrode chronoamperometry measurement of O_2 reduction at 0.0 V of a GC disk in a **Cu_2(btmpa)** solution (bottom panel, A). The disk current had 4 minute intervals of 0.8 V every 20 minutes according to the scheme in the top panel to be able to strip accumulated Cu^0. The Faradaic efficiency for H_2O_2 is given in B. The black dots represent the Faradaic efficiency of the time window since the last H_2O_2 measurement. The disk was rotated at 1600 rpm in a 0.1 M phosphate buffer of pH 7 with 0.15 mM catalyst.

indicating that the interval procedure greatly enhances the Faradaic efficiency. With the long 4-minute intervals, this efficiency could be kept up to two hours after the start of the measurement and a total Faradaic efficiency of 65% percent was obtained.

After 2 hours, the Faradaic efficiency dropped with every measurement and during the last hour of the 8 hour measurement, only 18% Faradaic efficiency was obtained (Figure C.11 and Table C.1). The total Faradaic efficiency for the entire 7 hour measurement was 34% because of the high efficiency in the first 2 hours. Equally, the efficiency of the short interval experiment dropped after 1.5 hours. In the time window between 5 and 6 hours after the start of the experiment, the calculated Faradaic efficiency was negative. This calculated negative value is a result of an overall decrease in bulk H_2O_2 concentration in that time window and indicates that more H_2O_2 is over-reduced than that H_2O_2 is produced. The same effect was observed for the continuous measurement where it already started in the time window between 4 and 5 hours after the start of the measurement. In the last hour of the short-interval experiment, the interval time was increased to 4 minutes. As a result, the calculated Faradaic efficiency was positive again and the H_2O_2 bulk concentration raised again, which indicated that over-reduction was H_2O_2 was diminished. In addition, the long interval experiment (4 minute intervals) had no decrease in bulk H_2O_2 concentration at any point during the measurement, demonstrating the significance of the duration of the stripping interval.

Even the long stripping interval of 4 minutes did not completely prevent over-reduction after 2 hours of amperometry. We believe that this is due to a steady rise in the bulk H_2O_2 concentration during the measurement. The rate of H_2O_2 over-reduction by **Cu_2(btmpa)** will increase with increasing H_2O_2 concentration as pointed out earlier (Figure C.6). However, it is more likely that that the over-reduction is mostly caused by Cu^0 as this deposits in a faster rate at higher bulk H_2O_2 concentrations. The following observations support this. First of all, the Faradaic efficiency is consistently lower for measurements with shorter or no stripping intervals (Figure C.10) after 2 hours. Also, 2 hours after the start of the measurement, all interval measurements display steeply rising reductive currents during the 20 minute 0.0 V measurement but all fall back after the stripping interval. These observations point to the accumulation of a species on the electrode (Cu^0) that facilitates over-reduction during the 20-minute period which is subsequently stripped after the stripping interval. As mentioned before, **Cu_2(btmpa)** itself seems to be more reluctant to desorb from the surface at 0.8 V. Another observation is the enhancement of the steep increase in current when the H_2O_2 concentration is

manually spiked (Figure C.11). Moreover, this steep increase in current is mostly avoided when the formed H_2O_2 is intercepted. In fact, this was achieved with the 8.5 hour RRDE measurement as the Pt ring, while sensing H_2O_2, is actually continuously converting H_2O_2 back to O_2 thereby limiting H_2O_2 build-up (Figure C.9). To some extent, there is build-up of H_2O_2 in the solution, but the reductive disk current remained remarkably constant over the course of 8 hours as opposed to the other measurements and remained close to the theoretical diffusion limited current of −0.49 mA for O_2 to H_2O_2 reduction. Furthermore, the ring current measurements did indicate that H_2O_2 selectivity remained high throughout the measurement. We therefore conclude that the decrease in Faradaic efficiency after 2 hours is caused by higher rates of Cu^0 deposition induced by a higher H_2O_2 concentration.

The faster deposition rate of Cu^0 after two hours as compared to the start of the measurement might be related to a faster rate of complex degradation. The catalyst-containing electrolyte slowly changes color from blue to green throughout the measurement (Figure C.1B). The same spectral changes in the UV-vis spectrum of the electrolyte could be replicated by adding 1.1 mM H_2O_2 to a 0.15 mM **Cu_2(btmpa)** solution in phosphate buffer (Figure C.1A). Monitoring the UV-vis spectrum over the course of a week showed that the low-intensity absorption at 675 nm remained but a second absorption appears at 359 nm. While this peak increased, another peak at 288 nm decreased and an isosbestic point at 298 nm was observed in between. Since the spectrum only changes upon the addition of H_2O_2 (Figure C.1C), the possibility of H_2O_2 coordination to **Cu_2(btmpa)** was further explored. The absorption at 359 nm could indicate a μ-η^2:η^2-peroxodicopper(II) structure.[54] Typically, complexes and enzymes with such a side-on peroxo dinuclear copper center have a high intensity absorption between 320 and 380 nm as well as a low intensity absorption between 520 and 610 nm. Both absorptions are ascribed to $\pi^* \rightarrow d_{xy}$ peroxo to Cu^{II} charge transfers.[55-58] The band at 610 nm in that case is most likely is obscured by the 675 nm absorption of unreacted **Cu_2(btmpa)**. The possibility of this core was further investigated by Raman spectroscopy (Figure C.12). A low energy O–O stretching band is typically observed for this core in the range of 730 – 760 cm^{-1}.[54-58] A broad signal at 760 cm^{-1} could be observed, but was also observed in the absence of H_2O_2. Since the Raman spectra with and without H_2O_2 overlap, no evidence for the presence O–O or Cu–O bonds was found. Therefore, the color and spectral changes are most likely due to ligand degradation by oxidation. This would in turn facilitate Cu^0 deposition, especially at higher H_2O_2 concentration. Overall, to achieve a high Faradaic efficiency for a longer period of time the produced H_2O_2 has to be intercepted to prevent Cu^0 deposit, and any formed deposit has to be

stripped of electrochemically. We have shown that the latter approach resulted in a Faradaic efficiency between 60 and 70% for up to 2 hours for the production of H_2O_2.

4.3 Conclusion

The dinuclear copper complex **Cu_2(btmpa)** is able to catalyze the electrochemical O_2 reduction with H_2O_2 as major product. Reduction and re-oxidation of the complex is accompanied by slow electron transfer due to geometrical constrains that are absent in the mononuclear **Cu(tmpa)** complex. That way, the rate of O_2 reduction of **Cu_2(btmpa)** is lower, and, more importantly, the over-reduction of H_2O_2 is largely blocked. The complex produces H_2O_2 with a high Faradaic efficiency of 60 to 70% at 0.0 V over the course of 2 hours. Cu^0 deposition lowers the Faradaic efficiency, but can be counteracted by briefly applying a stripping potential periodically. Additionally, the catalytic activity increases significantly in the first half hour of chronoamperometry and the current can stabilize close to the theoretical diffusion limited current for O_2 to H_2O_2 reduction when H_2O_2 is intercepted. Potential dependent accumulation of the catalyst in its reduced dicopper(I) state on the glassy carbon electrode is the most likely explanation for this initial fast increase in activity. This is the first extensive study for prolonged electrochemical O_2 to H_2O_2 reduction by a molecular catalyst. We have successfully identified that fine-tuning the potential, the use of Cu^0 stripping intervals, and applying methods to intercept the formed H_2O_2 can significantly improve the Faradaic efficiency. Thereby, we have been able to put the intrinsic high H_2O_2 selectivity of **Cu_2(btmpa)** to use. We anticipate that our results will allow for the next step, which is the incorporating the catalyst in devices for the direct electrochemical production of H_2O_2 from O_2.

4.4 Acknowledgements

Dr. Andrey Konovalov and the Competence Center in Magnetometry at institut Jean Lamour in Nancy are kindly thanked for the measurement, simulation and interpretation of the SQUID data. Max Makurat is kindly thanked for the measurement of the Raman spectra. This work has been financially supported by the European Research Council (ERC starting grant 637556 Cu4Energy to dr. D. G. H. Hetterscheid).

4.5 Experimental

4.5.1 General

All chemicals were bought from commercial suppliers and used as received without further purification. The pH was measured with a Hannah Instruments HI 4222 pH meter that was calibrated with five IUPAC standard buffers. UV-vis measurements were performed on a Varian Cary 50 UV-vis spectrometer. ^{1}H NMR measurements were performed with a Bruker DPX-300 spectrometer using deuterated solvents obtained from Eurisotop. $CDCl_3$ was purified by filtration over basic alumina before use. All chemical shifts (δ) are reported with respect to the solvent peak.[59] Elemental analysis was performed by Mikroanalytisch Laboratorium Kolbe in Oberhausen, Germany. Mass spectra were recorded on a Thermo Fisher Scientific MSQ Plus ESI. EPR spectra were recorded on a Bruker EMXplus X-band spectrometer. Reflectance Raman spectra were recorded with a WITech alpha 300 R confocal Raman microscope equipped with a 532 nm laser (1 mW). A 100 x objective with a numeral aperture of 0.9 was used (Zeiss). For preparation of the sample, an aqueous solution of 3 mM **Cu_2(btmpa)** and 22 mM H_2O_2 was dropcasted on a Si/SiO_2 wafer (Siegert wafer) with a native silicon oxide layer of 285 nm. SQUID measurements were performed on a Quantum Design MPMS-XL 7T SQUID magnetometer employing the settle approach with activated No-overshoot mode om the 300-2K temperature range with varying increment: 5K (300-150K), 2K (150-50K), 1K (50-25K), and 0.5K (25-2K) at constant 5 kOe magnetic field. An automatic diamagnetic correction was applied for a sample holder that was measured separately beforehand. Each data point was averaged over 4 consecutive scans.

4.5.2 Synthesis

Synthesis of 6,6'-bis(hydroxymethyl)-2,2'-bipyridine (3)

3 (Scheme 4.1) was synthesized with **2** as crude intermediate. **2** was synthesized following the procedure for synthesizing the methyl ester adapted from Forato *et al.*[60] ethanol (EtOH) instead of methanol (MeOH) was used to prepare the ethyl ester. 803.7 mg (3.29 mmol) of 2,2'-bipyridine-6,6'-carboxylic acid (ChemCruz, **1**) was loaded into a dry flask under inert atmosphere. 120 ml degassed EtOH (99.8%, Riedel-de Haën) was added to dissolve the compound. 16 ml of H_2SO_4 (98%, VWR) was added drop-wise over the course of 10 min. The mixture was set to reflux overnight. After cooling the mixture to 0 °C, it was slowly poured into 150 ml of saturated $NaHCO_3$ solution. The resulting mixture was extracted using 4 x 100 ml

DCM (dichloromethane, Honeywell, >99.9%). The organic layers were collected, and the solvent was evaporated under reduced pressure resulting in a crude white solid which was characterized by ^{1}H NMR and ESI MS. Besides peaks belonging to **2**, the monosubstituted by-product was found as well. This and other impurities were removed in the next step of the synthesis. ESI MS of **2** *m/z* (found (calculated)): 301.1 (301.3 [M + H$^+$]); 323.1 (323.3 [M + Na$^+$]). ^{1}H NMR of **2** (300 MHz, $CDCl_3$) δ 8.88 (dd, 2H, ^3J(H,H) = 7.9 Hz, ^4J(H,H) = 1.1 Hz, Py-NCC-Py-C*H*), 8.21 (dd, 2H, ^3J(H,H) = 7.8 Hz, ^4J(H,H) = 1.1 Hz), 7.99 (t, 2H, ^3J(H,H) = 7.8 Hz), *p*-Py-*H*), 4.53(q, 4H, ^3J(H,H) = 7.1 Hz, CH_3CH_2); 1.49 (t, 6H, ^3J(H,H) = 7.1 Hz, CH_3CH_2).

The crude product **2** was further used to synthesize **3** without further purification. **3** was synthesized following the procedure by Ganesan *et al.*[61] 1.1561 g of **2** was dissolved in 40 ml of dry, degassed THF (tetrahydrofuran, Sigma Aldrich) and loaded into a dry flask with inert atmosphere. The solution was further degassed using an N_2 flow for 30 min. 1.464 g (38.7 mmol) of $NaBH_4$ (Aldrich) was added to this solution. 9 ml of dry, degassed MeOH (Honeywell, >99.9%) was dropwise added by syringe, resulting in the formation of a large amount of gas. Once the gas production stopped, the mixture was set to reflux overnight. 150 ml of saturated NH_4Cl solution, prepared using NH_4Cl (Honeywell) and demineralized water, was

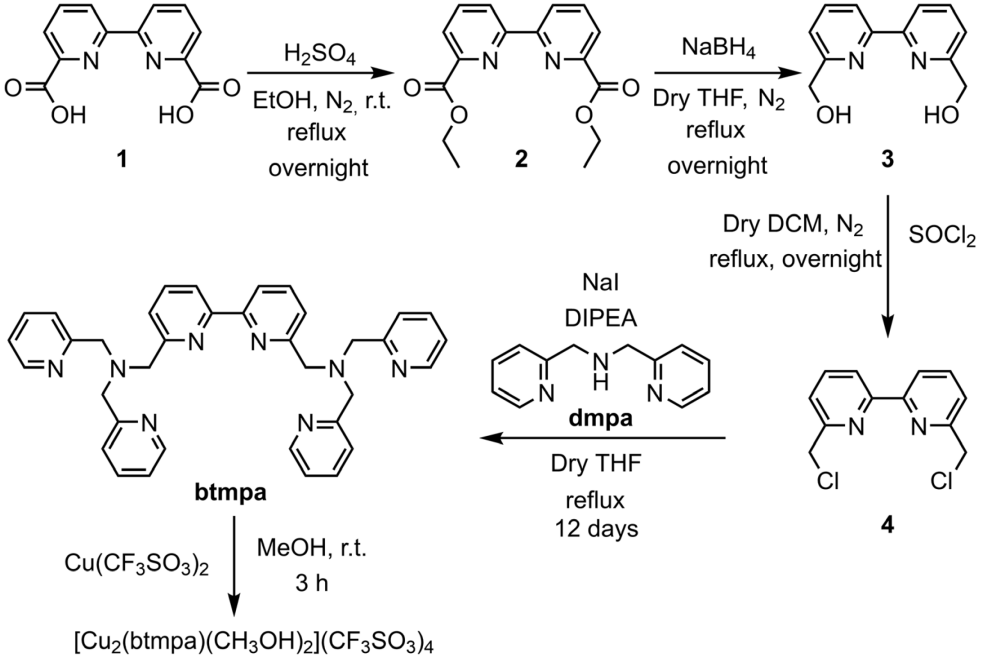

Scheme 4.1. Synthesis of btmpa and $[Cu_2(btmpa)(CH_3OH)_2](CF_3SO_3)_4$.

added to the reaction mixture to neutralize the remaining $NaBH_4$. The resulting mixture was extracted using 3 x 100 ml EtOAc (ethyl acetate, VWR, Rectapur®). The organic layers were collected, and the solvent was evaporated under reduced pressure. 687.8 mg of product was obtained in the form of a white/yellow solid (3.18 mmol, 97% yield with respect to **1**). ^{1}H NMR matches the values reported by Ganesan *et al.*[61] within 0.2 ppm. ESI MS *m/z* (found (calculated)): 217.0 (217.1 [M + H^+]); 239.0 (239.1 [M + Na^+]). ^{1}H NMR (300 MHz, $CDCl_3$) δ 8.41 (dd, 2H, ^3J(H,H) = 7.8 Hz, ^4J(H,H) = 1.0 Hz, Py-NCC-Py-C*H*), δ 7.87 (t, 2H, ^3J(H,H) = 7.8 Hz, *p*-Py-*H*), δ 7.52 (dd, 2H, ^3J(H,H) = 7.8 Hz, ^4J(H,H) = 1.0 Hz, Py-NCC-OH-C*H*), 4.77 (s, 4H, CH_2).

Synthesis of 6,6'-bis(chloromethyl)-2,2'-bipyridine (4)

687.8 mg of **3** was dissolved in 60 ml of dry, degassed DCM (Sigma Aldrich) and loaded into a dry flask with inert atmosphere. The resulting solution was further degassed by purging with N_2 for 30 min. 1.2 ml of $SOCl_2$ (Acros Organics) was added dropwise, resulting in a turbid yellow solution. After stirring for 15 minutes the solution had turned clear and yellow. The mixture was left to stir under reflux overnight. After attaching a gas trap filled with 40 ml 10 M NaOH solution, 100 ml of water was carefully added to the reaction mixture to neutralize the remaining $SOCl_2$. The mixture was left stirring vigorously for 1 h to allow the $SOCl_2$ to neutralize completely. The reaction mixture was extracted using DCM (3 x 100 ml). The organic layers were collected, and the solvent was evaporated under reduced pressure resulting in a yellow solid. 643.8 mg of product was obtained (2.54 mmol, 80% yield). The recorded ^{1}H NMR spectrum matches reported values with a maximum 0.05 ppm deviation.[62, 63] MS *m/z* (found (calculated)): 252.9 (253.1 [M + H^+]). ^{1}H NMR (300 MHz, $CDCl_3$) δ 8.41 (dd, 2H, ^3J(H,H) = 7.9 Hz, ^4J(H,H) = 1.0 Hz, Py-NCC-Py-C*H*), δ 7.87 (t, 2H, ^3J(H,H) = 7.8 Hz, *p*-Py-*H*), 7.52 (dd, 2H, ^3J(H,H) = 7.7 Hz, ^4J(H,H) = 1.0 Hz, Py-NCC-Cl-C*H*), 4.77 (s, 4H, CH_2)

Synthesis of 6,6'-bis(2,2'-dipicolylamine)-2,2'-bipyridine (btmpa)

Synthesis and initial purification

465.1 mg of **4** and 16.4 mg of NaI were loaded into a dry flask attached to a Schlenk setup. The solids were degassed and subsequently dissolved in 80 ml Degassed, dry THF. 3.2 ml DIPEA (N,N-diisopropylethylamine, Sigma Aldrich) and 0.66 ml 2,2'-dipicolylamine (dmpa, Chemodex) were added to the solution. The resulting yellow solution was refluxed for 12 days, while the progress was checked by

NMR. After 12 days, 200 ml of saturated $NaHCO_3$ solution was added followed by an extraction using 4 x 100 ml DCM. The organic layers were collected, and all volatiles were evaporated under reduced pressure. A silica column (Silica gel 40 – 63 μm, 60 Å, Screening Devices) using a gradient eluent of 0-10% MeOH in DCM was performed as a first purification. Column chromatography alone was not enough to remove unreacted dmpa since it has a very similar Rf value as btmpa and both compounds suffer from tailing and thus mixing. From several recrystallization attempts from 2 : 3 DCM : Et_2O (diethyl ether, Honeywell), part of the crude product could be purified and btmpa was obtained as white crystals. 113.9 mg (0.197 mmol) of btmpa was obtained as first batch.

Purification with hexanoic anhydride

As mentioned, unreacted dmpa is hard to remove from btmpa because the Rf values are very similar and both compounds tail slightly on alumina and largely on silica columns. A large difference in Rf would help to avoid mixing due to tailing of the compounds. Therefore, hexanoic anhydride (Sigma Aldrich) was used to change the Rf of dmpa. This method is based on the reaction of the secondary amine of dmpa with the anhydride to obtain an amide. The aliphatic tail of the amide makes the impurity more hydrophobic and, as a result, increases its Rf value with respect to that of btmpa. btmpa itself has no primary or secondary amines that can react with the anhydride. This way the compounds could be purified successfully. Specifically, 140 mg crude product containing btmpa, which was left after the first purification by column chromatography, was dissolved in 5 ml dry DCM (Sigma Aldrich), 135 μL DIPEA and 60 μL hexanoic anhydride (Sigma Aldrich) were added to the solution. The reaction mixture was stirred at room temperature for 2.5 hours. Next, the mixture was neutralized by adding 1 M HCl till the pH reached 7. The crude mixture was separated in two layers and the aqueous layer was extracted 3 times with DCM. All organic layers were combined, dried over Na_2SO_4 and filtered. All volatiles were removed under reduced pressure. For the purification, the product was dissolved in DCM and loaded on an alumina column (Brockmann Type 1 Basic alumina). A gradient eluent was used from 0.2% triethylamine to 0.5% with additional 0.1% MeOH in DCM. The product fractions were washed with a saturated $NaHCO_3$ solution. Subsequently, this $NaHCO_3$ solution was extracted 3 times with DCM. All organic fractions were combined, dried over Na_2SO_4, and filtered before the volatiles were removed under reduced pressure. The obtained white solid was washed twice with pentane and once with Et_2O. After drying, 108 mg (0.187 mmol) of btmpa was

obtained. ^{1}H NMR and MS confirmed the presence of btmpa and the absence of dmpa and hexanoic amide. The ^{1}H NMR spectra matches reported spectra.[46] The total yield of pure product is 241.9 mg (0.418 mmol, 23%). ESI MS *m/z* (found (calculated)): 601.5 (601.28 [M + Na^+]); 579.5 (579.3, [M + H^+]); 290.3 (290.15, [M + 2 H^+]). ^{1}H NMR (300 MHz, $CDCl_3$) δ 8.53 (dt, 4H, ^{3}J(H,H) = 4.9 Hz, ^{4}J(H,H) = 1.4 Hz, *o*-Py-*H*), 8.30 (dd, 2H ^{3}J(H,H) = 7.8 Hz, ^{4}J(H,H) = 1.1 Hz, Py-NCC-Py-C*H*), 7.77 (t, 2H, ^{3}J(H,H) = 7.7 Hz, *p*-biPy-*H*), 7.72 – 7.58 (m, 8H, *p*-Py-*H* and *m*-Py-*H*), 7.54 (dd, 2H, ^{3}J(H,H) = 7.7 Hz, ^{4}J(H,H) = 1.1 Hz, biPy-NCCN-C*H*), 7.14 (m, 4H, Py-NCHCH$_2$N-C*H*), 3.95 (overlapping singlets, 12H, CH_2).
In total, both batches (113.9 and 108 mg) gave a total yield of 221.9 mg (0.383 mmol, 21%).

Synthesis of $[Cu_2(btmpa)(CH_3OH)_2](CF_3SO_3)_4$ (Cu_2(btmpa))

108 mg of **btmpa** was dissolved in 5 ml MeOH yielding a yellow solution. Next, 136 mg of Cu(II)$(CF_3SO_3)_2$ (Alfa Aesar) was dissolved in 1 ml MeOH and added to the ligand solution. The solution turned from green to dark blue upon addition. The mixture was stirred for 3 hours at room temperature after which the solvent was removed under reduced pressure. The remaining solid residue was redissolved in 2 ml MeOH and Et_2O was slowly added by vapor diffusion at 4 °C temperature. The obtained blue crystals were filtered and washed with cold Et_2O and dried. After repeating the crystallization, 162 mg (0.118 mmol, 63%) blue crystals of the complex were obtained. The calculated (%) elemental analysis ratio (%) for $[Cu_2(btmpa)(MeOH)_2](OTf)_4$ ($C_{42}H_{42}Cu_2N_8O_{14}S_4$) + 2.5 H_2O : C 35.75, H 3.36, N 7.94; found: C 35.48, H 3.10, N 7.78. UV-vis λ_{max}: 228 nm, 675 nm (0.15 mM in water); 632 nm, 816 nm (2.0 mM in MeCN). EPR 0.6 mM in H_2O: $g_{||}$ = 2.21, $g_{\perp}$ = 2.08; phosphate buffer: $g_{||}$ = 2.23, $g_{\perp}$ = 2.06; in dimethyl formamide: $g_{||}$ = 2.23 (A_{Cu} = 500 Hz), $g_{\perp}$ = 2.06. (Figure C.2).

4.5.3 General electrochemistry

For all aqueous solutions, all experiments and for cleaning of glassware Milli-Q grade Ultrapure water (>18.2 MΩ cm resistivity) was used unless mentioned otherwise. The pH 7 electrolyte was prepared with NaH_2PO_4 (Merck Suprapur ©, 99.99%) and Na_2HPO_4 (Fluka Traceselect© 99.995%) with 0.1 M phosphate strength. Electrochemical experiments were performed with a three-electrode setup in a custom-made, single-compartment glass cell. For EQCM, RRDE and bulk electrolysis, special cells were used that are described separately. Autolab PGSTAT 12, 204, 128N and IVIUM CompactStat potentiostats were used in combination with

NOVA 2.1 or IVIUM software. All glassware used for electrochemistry was cleaned by boiling in and copiously rinsing the glassware with water prior to each experiment. Periodically and before each RRDE measurement, the glassware was cleaned by immersing the glassware in a 1 g/l $KMnO_4$ solution in 0.5 M H_2SO_4 (Sigma, reagent grade) overnight. Afterwards, the glassware was rinsed 5–10 times with water. To re-oxidize any MnO_2 traces, water, a few drops of H_2O_2 (Merck Emprove, 35%) and H_2SO_4 (Merck) were added. Finally, the glassware was rinsed 5-10 times and boiled in water for a total of three times

All electrolytes solutions were purged by argon (Linde, Ar 5.0) prior to each experiment for at least 30 minutes and the cell was kept under a flow of argon during the experiment. For experiments under O_2 (Linde, O_2 5.0), the electrolyte was purged with O_2 for at least 10 minutes prior to the measurement and was purged continuously during RRDE measurements.

In all cases, the reference electrode was the reversible hydrogen electrode by utilizing a platinum mesh in H_2 (Linde, H_2 5.0) saturated electrolyte that is operated at the same pH as the working electrode or by using a HydroFlex (Gaskatel). The cell and reference electrode are connected via a Luggin capillary. The counter electrode was a large surface area gold wire that was flame annealed prior to use. The working electrode was glassy carbon (GC, Metrohm, 0.07 cm^2) encapsulated in PEEK (polyether ether ketone). The GC electrode was polished before each measurement. Either manual or mechanical polish methods were used. Manual polishing was applied with 1.0, 0.3 and 0.05 micron alumina slurry (Buehler) on MicroCloth (Buehler) polishing cloths for 2 minutes followed by rinsing and sonicating the electrode in water for 10 minutes. Mechanical polishing was applied with a Labopol-20 polishing machine on Dur type polishing cloths with 1.0 micron diamond and 0.04 micron silica suspensions for 1 minute (Struers). After the diamond polishing, the electrode was rinsed with water and 2-propanol to remove the oily substances from the slurry. The silica polish was followed by a rinse with water. After that, the electrode was sonicated in water for 10 minutes.

4.5.4 EQCM

EQCM experiments were performed with an Autolab gold EQCM electrode (0.35 cm^2) that consist of a 200 nm thick gold layer deposited on a quartz crystal. An adjusted Autolab PEEK EQCM cell was used that was able to contain up to 5 ml of electrolyte.

4.5.5 RRDE

RRDE experiments were performed in a three electrode setup with custom-made two-compartment cells that could separate the working electrodes from the counter electrode via a water permeable glass frit. A glassy carbon disk (0.196 cm^2) surrounded by a platinum ring in a ChangeDisk configuration was used in a Pine MSR rotator as supplied by Pine Instruments. The GC disk and Pt ring electrodes were, prior to each measurement, separately polished. Both were either manually or mechanically polished. For the GC disk, the same procedure for the PEEK encapsulated disk was used. For Pt, the manual polish was performed with 1.0 and 0.3 micron alumina for 30 seconds and 0.05 micron alumina for 1 minute after which the electrode was sonicated for 10 minutes in water. The mechanical polish was equal to the treatment for the GC disk. When applicable, the Pt ring was further electropolished by performing CV in 0.1 M phosphate buffer of pH 7 for 50 scans at a 500 mV/s scan rate between 1.7 and –0.1 V while the shaft was rotated at 1600 rpm.

4.5.6 Bulk electrolysis and Faradaic efficiency

The Faradaic efficiency was determined by bulk electrolysis in combination with H_2O_2 enzyme based photometric determination of the bulk H_2O_2 concentration with the Reflectoquant® system (Merck) using test strips for 0.2 to 20 mg/l H_2O_2 (Merck). The bulk electrolysis was performed in a custom-made glass cell with glass-frit separated compartments for the reference, work and counter electrode. A HydroFlex (Gaskatel) reference electrode was used as RHE reference. The counter electrode was a high surface area gold wire. The work electrode was a custom-made, mechanically polished GC electrode (0.196 cm^2) in a rotating disk setup from Pine. The electrode was continuously rotated at 1600 rpm. The initial volume of the 0.15 mM **Cu_2(btmpa)** solution was 33.6 ml. A circa 1.5 ml aliquot was taken for each H_2O_2 measurement and weighed to correct for the decrease in volume of the bulk solution during the measurement. Each aliquot was tested at least twice with the test strips immediately after removing it from the solution. The theoretical charge required to obtain the measured concentration difference of H_2O_2 in the time between two measurements was calculated. The actual charge that passed in the same time window was obtained by integration of the current over time.

4.6 References

1. *Hydrogen Peroxide*; 18; Global Industry Analysts: 2020.
2. Eul, W.; Moeller, A.; Steiner, N., Hydrogen Peroxide. In *Kirk-Othmer Encyclopedia of Chemical Technology* [Online] John Wiley & Sons, Inc.: 2000. http://dx.doi.org/10.1002/0471238961.0825041808051919.a01.pub2.
3. Hage, R.; Lienke, A., *Angew. Chem. Int. Ed.* **2006,** *45*, 206–222.
4. Süss, H. U., Bleaching. In *Ullmann's Encyclopedia of Industrial Chemistry*, 2012.
5. Legrini, O.; Oliveros, E.; Braun, A. M., *Chem. Rev.* **1993,** *93*, 671–698.
6. Metcalf & Eddy Inc.; Tchobangolous, G., *Wastewater Engineering: Treatment and Resource Recovery*. 5th edition ed.; Mcgraw-Hill Education: 2014.
7. Goor, G., *Catalytic Oxidations with Hydrogen Peroxide as Oxidant*. Kluwer Academic Publishers: The Netherlands, 1992.
8. Campos-Martin, J. M.; Blanco-Brieva, G.; Fierro, J. L. G., *Angew. Chem. Int. Ed.* **2006,** *45*, 6962–6984.
9. Berl, E., *Trans. Electrochem. Soc.* **1939,** *76*, 359.
10. Xia, C.; Xia, Y.; Zhu, P.; Fan, L.; Wang, H., *Science* **2019,** *366*, 226.
11. Jiang, Y.; Ni, P.; Chen, C.; Lu, Y.; Yang, P.; Kong, B.; Fisher, A.; Wang, X., *Adv. Energy Mater.* **2018,** *8*, 1801909.
12. Siahrostami, S.; Verdaguer-Casadevall, A.; Karamad, M.; Deiana, D.; Malacrida, P.; Wickman, B.; Escudero-Escribano, M.; Paoli, E. A.; Frydendal, R.; Hansen, T. W.; Chorkendorff, I.; Stephens, I. E. L.; Rossmeisl, J., *Nat. Mater.* **2013,** *12*, 1137–1143.
13. Verdaguer-Casadevall, A.; Deiana, D.; Karamad, M.; Siahrostami, S.; Malacrida, P.; Hansen, T. W.; Rossmeisl, J.; Chorkendorff, I.; Stephens, I. E. L., *Nano Lett.* **2014,** *14*, 1603–1608.
14. Jirkovský, J. S.; Panas, I.; Ahlberg, E.; Halasa, M.; Romani, S.; Schiffrin, D. J., *J. Am. Chem. Soc.* **2011,** *133*, 19432–19441.
15. Song, C.; Zhang, J., Electrocatalytic Oxygen Reduction Reaction. In *PEM Fuel Cell Electrocatalysts and Catalyst Layers: Fundamentals and Applications*, Zhang, J., Ed. Springer London: London, 2008; pp 89–134.
16. Chen, S.; Chen, Z.; Siahrostami, S.; Kim, T. R.; Nordlund, D.; Sokaras, D.; Nowak, S.; To, J. W. F.; Higgins, D.; Sinclair, R.; Nørskov, J. K.; Jaramillo, T. F.; Bao, Z., *ACS Sustainable Chem. Eng.* **2018,** *6*, 311–317.
17. Liu, Y.; Quan, X.; Fan, X.; Wang, H.; Chen, S., *Angew. Chem. Int. Ed.* **2015,** *54*, 6837–6841.
18. Kim, H. W.; Ross, M. B.; Kornienko, N.; Zhang, L.; Guo, J.; Yang, P.; McCloskey, B. D., *Nat. Catal.* **2018,** *1*, 282–290.
19. Lu, Z.; Chen, G.; Siahrostami, S.; Chen, Z.; Liu, K.; Xie, J.; Liao, L.; Wu, T.; Lin, D.; Liu, Y.; Jaramillo, T. F.; Nørskov, J. K.; Cui, Y., *Nat. Catal.* **2018,** *1*, 156–162.
20. Iglesias, D.; Giuliani, A.; Melchionna, M.; Marchesan, S.; Criado, A.; Nasi, L.; Bevilacqua, M.; Tavagnacco, C.; Vizza, F.; Prato, M.; Fornasiero, P., *Chem* **2018,** *4*, 106–123.
21. Chen, S.; Chen, Z.; Siahrostami, S.; Higgins, D.; Nordlund, D.; Sokaras, D.; Kim, T. R.; Liu, Y.; Yan, X.; Nilsson, E.; Sinclair, R.; Nørskov, J. K.; Jaramillo, T. F.; Bao, Z., *J. Am. Chem. Soc.* **2018,** *140*, 7851–7859.
22. Han, L.; Sun, Y.; Li, S.; Cheng, C.; Halbig, C. E.; Feicht, P.; Hübner, J. L.; Strasser, P.; Eigler, S., *ACS Catal.* **2019,** *9*, 1283–1288.
23. Fellinger, T.-P.; Hasché, F.; Strasser, P.; Antonietti, M., *J. Am. Chem. Soc.* **2012,** *134*, 4072–4075.
24. Fukuzumi, S.; Yamada, Y.; Karlin, K. D., *Electrochim. Acta* **2012,** *82*, 493–511.
25. Fukuzumi, S.; Lee, Y.-M.; Nam, W., *ChemCatChem* **2018,** *10*, 9–28.
26. Pegis, M. L.; Wise, C. F.; Martin, D. J.; Mayer, J. M., *Chem. Rev.* **2018,** *118*, 2340–2391.
27. Nagao, K.; Hiroshi, S.; Tetsuo, O., *Chem. Lett.* **1985,** *14*, 1917–1920.
28. He, Q.; Mugadza, T.; Hwang, G.; Nyokong, T., *Int. J. Electrochem. Sci.* **2012,** *7*, 7045–7064.
29. Kuwana, T.; Fujihira, M.; Sunakawa, K.; Osa, T., *J. Electroanal. Chem. Interfacial Electrochem.* **1978,** *88*, 299–303.
30. Bettelheim, A.; Kuwana, T., *Anal. Chem.* **1979,** *51*, 2257–2260.
31. Costentin, C.; Dridi, H.; Savéant, J.-M., *J. Am. Chem. Soc.* **2015,** *137*, 13535–13544.
32. Kobayashi, N.; Nishiyama, Y., *J. Phys. Chem.* **1985,** *89*, 1167–1170.
33. Langerman, M.; Hetterscheid, D. G. H., *Angew. Chem. Int. Ed.* **2019,** *58*, 12974–12978.
34. Chan, R. J. H.; Su, Y. O.; Kuwana, T., *Inorg. Chem.* **1985,** *24*, 3777–3784.
35. D'Souza, F.; Deviprasad, R. G.; Hsieh, Y.-Y., *J. Electroanal. Chem.* **1996,** *411*, 167–171.
36. D'Souza, F.; Hsieh, Y.-Y.; Deviprasad, G. R., *J. Electroanal. Chem.* **1997,** *426*, 17–21.

37. Geiger, T.; Anson, F. C., *J. Am. Chem. Soc.* **1981,** *103*, 7489–7496.
38. Kang, C.; Anson, F. C., *Inorg. Chem.* **1995,** *34*, 2771–2780.
39. Smith, P. T.; Kim, Y.; Benke, B. P.; Kim, K.; Chang, C. J., *Angew. Chem. Int. Ed.* **2020,** *59*, 4902–4907.
40. Jacobson, R. R.; Tyeklar, Z.; Farooq, A.; Karlin, K. D.; Liu, S.; Zubieta, J., *J. Am. Chem. Soc.* **1988,** *110*, 3690–3692.
41. Tyeklár, Z.; Jacobson, R. R.; Wei, N.; Murthy, N. N.; Zubieta, J.; Karlin, K. D., *J. Am. Chem. Soc.* **1993,** *115*, 2677–2689.
42. Haber, F.; Weiss, J.; Pope, W. J., *Proc. R. Soc. London, Ser. A* **1934,** *147*, 332–351.
43. Garcia-Bosch, I.; Cowley, R. E.; Díaz, D. E.; Siegler, M. A.; Nam, W.; Solomon, E. I.; Karlin, K. D., *Chem. - Eur. J.* **2016,** *22*, 5133–5137.
44. Døssing, A. H., Alan; Toftlund, H., *Acta Chem. Scand.* **1996,** *50*, 95–101.
45. Dürr, H.; Zengerle, K.; Trierweiler, H.-P., *Z. Naturforsch. B* **1988,** *43*, 361–368.
46. Lee, D.-H.; Murthy, N. N.; Karlin, K. D., *Inorg. Chem.* **1997,** *36*, 5785–5792.
47. Lim, B. S.; Holm, R. H., *Inorg. Chem.* **1998,** *37*, 4898–4908.
48. Marcus, R. A., *Rev. Mod. Phys.* **1993,** *65*, 599–610.
49. Schley, N. D.; Blakemore, J. D.; Subbaiyan, N. K.; Incarvito, C. D.; D'Souza, F.; Crabtree, R. H.; Brudvig, G. W., *J. Am. Chem. Soc.* **2011,** *133*, 10473–10481.
50. van der Ham, C. J. M.; Işık, F.; Verhoeven, T. W. G. M.; Niemantsverdriet, J. W.; Hetterscheid, D. G. H., *Catal. Today* **2017,** *290*, 33–38.
51. van Dijk, B.; Hofmann, J. P.; Hetterscheid, D. G. H., *Phys. Chem. Chem. Phys.* **2018,** *20*, 19625–19634.
52. van Dijk, B.; Rodriguez, G. M.; Wu, L.; Hofmann, J. P.; Macchioni, A.; Hetterscheid, D. G. H., *ACS Catal.* **2020,** *10*, 4398–4410.
53. Hall, S. B.; Khudaish, E. A.; Hart, A. L., *Electrochim. Acta* **1998,** *43*, 579–588.
54. Mirica, L. M.; Ottenwaelder, X.; Stack, T. D. P., *Chem. Rev.* **2004,** *104*, 1013–1046.
55. Kitajima, N.; Moro-oka, Y., *Chem. Rev.* **1994,** *94*, 737–757.
56. Ross, P. K.; Solomon, E. I., *J. Am. Chem. Soc.* **1990,** *112*, 5871–5872.
57. Ross, P. K.; Solomon, E. I., *J. Am. Chem. Soc.* **1991,** *113*, 3246–3259.
58. Solomon, E. I.; Tuczek, F.; Root, D. E.; Brown, C. A., *Chem. Rev.* **1994,** *94*, 827–856.
59. Fulmer, G. R.; Miller, A. J. M.; Sherden, N. H.; Gottlieb, H. E.; Nudelman, A.; Stoltz, B. M.; Bercaw, J. E.; Goldberg, K. I., *Organometallics* **2010,** *29*, 2176–2179.
60. Forato, F.; Belhboub, A.; Monot, J.; Petit, M.; Benoit, R.; Sarou-Kanian, V.; Fayon, F.; Jacquemin, D.; Queffelec, C.; Bujoli, B., *Chem. - Eur. J.* **2018,** *24*, 2457–2465.
61. Ganesan, V.; Sivanesan, D.; Yoon, S., *Inorg. Chem.* **2017,** *56*, 1366–1374.
62. Li, W.; Xie, J.-H.; Yuan, M.-L.; Zhou, Q.-L., *Green Chem.* **2014,** *16*, 4081–4085.
63. Newkome, G. R.; Kohli, D. K.; Fronczek, F., *J. Chem. Soc., Chem. Commun.* **1980**, 9–11.